

Creating Materials and Energy Solutions

Computational and Experimental Development of Novel High Temperature Alloys

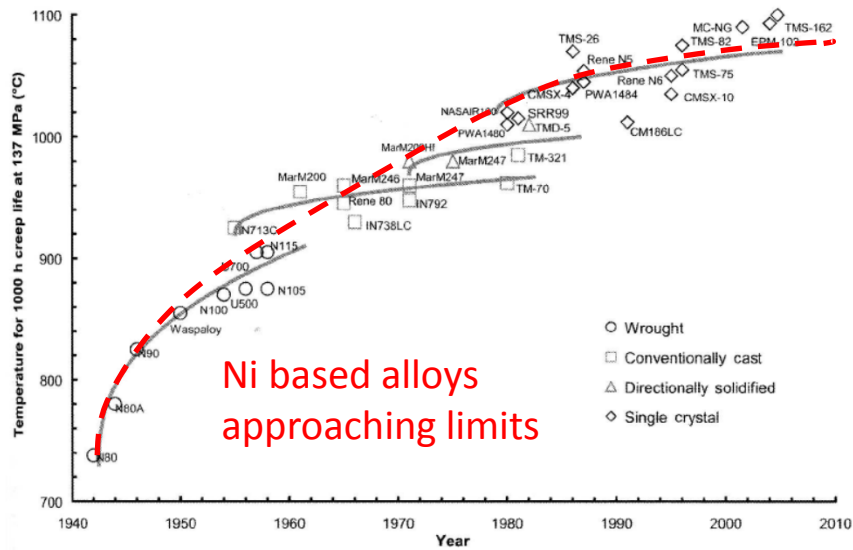
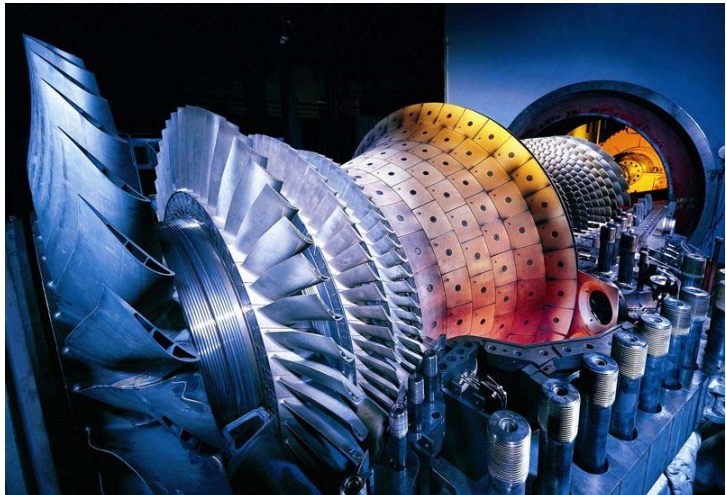
Matthew J. Kramer, Tyler R. Bell, Pratik K. Ray, Mufit Akinç
Prashant Singh, Linlin Wang and Duane D. Johnson

2015 Crosscutting Technology and Research Meeting
April 29, 2015

*This work was supported by the **DOE-FE (AMR program)** through Ames Laboratory contract no.
DE-AC02-07CH11358*



The High Temperature challenge



Higher temperatures → Higher energy efficiencies

Challenges –

- High T oxidation
- Moisture
- Creep and high T deformation
- Toughness & manufacturability
- Highly variable coal combustion environments

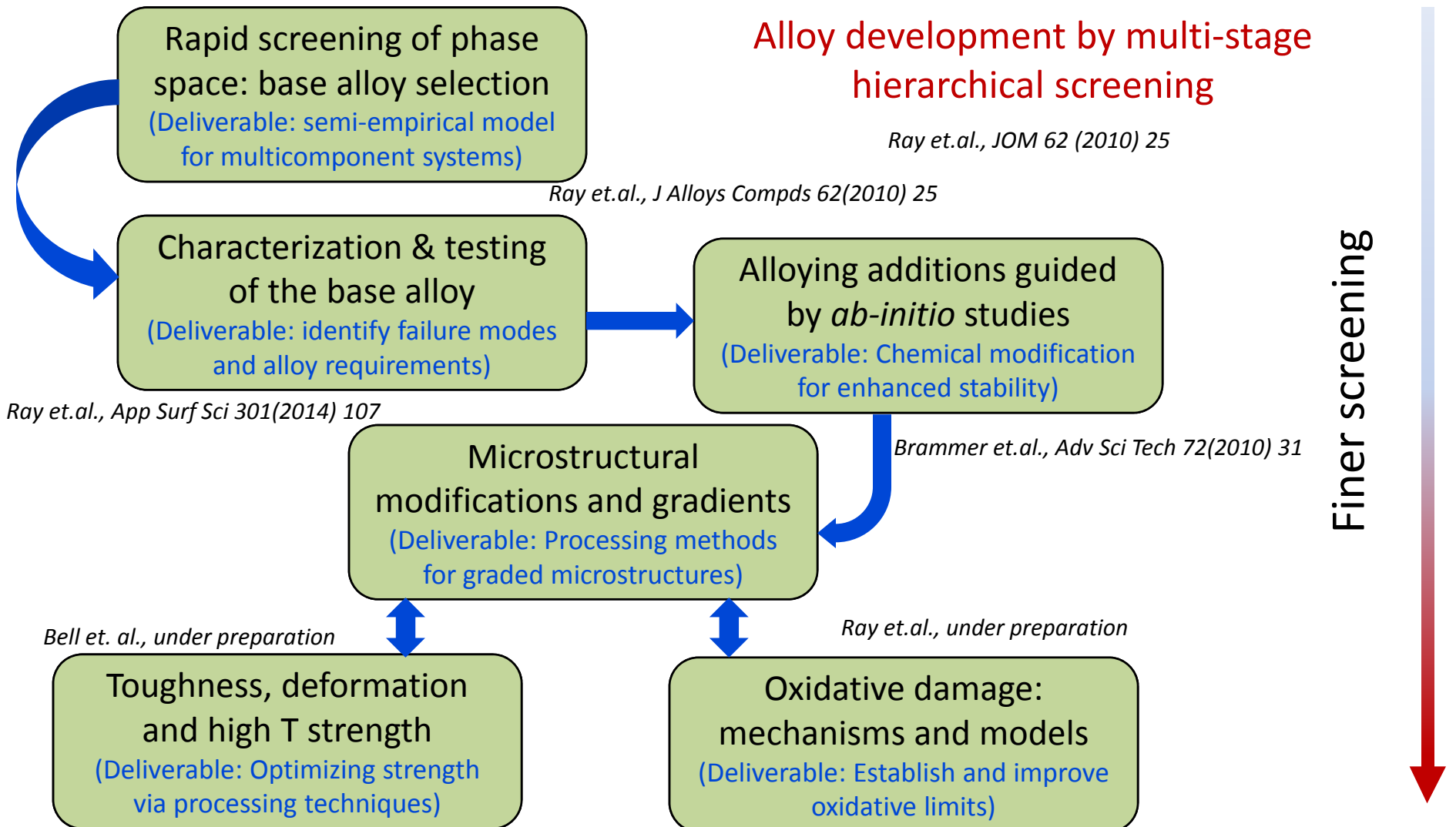
The problem:

- Are there effective ways of tweaking existing systems?
- Can we develop a new alloy system?

Key metrics:

- High melting temperatures
- Microstructural stability
- Toughness $\geq 20 \text{ MPa} \cdot \text{m}^{1/2}$
- Oxidative Stability

Conceptual approach



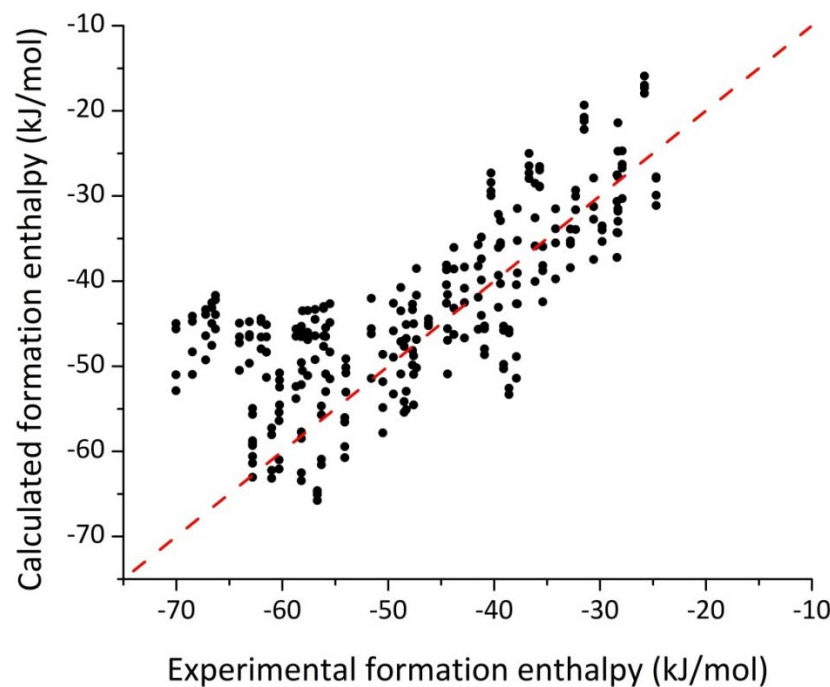
Enthalpies of multicomponent alloys

# of elements	Combinations
3	3160
4	82160
5	1.58×10^6
6	2.40×10^7

$$\Delta H = \phi_1 \Delta H_{AB}(\alpha) + \phi_2 \Delta H_{BC}(\beta) + \phi_3 \Delta H_{CA}(\gamma)$$

Individual binaries calculated using Miedema's equation

$$\Delta H = c_A c_B (f_B^A \Delta H_{AB}^{i/c} + f_A^B \Delta H_{BA}^{i/c})$$



$$\sum_{i=1}^3 \phi_i = 1$$

Mass balance constraints

$$\phi_1 \alpha + \phi_3 (1 - \gamma) = x_A$$

$$\phi_2 \beta + \phi_1 (1 - \alpha) = x_B$$

$$\phi_3 \gamma + \phi_2 (1 - \beta) = x_C$$

Ray et.al., J. Alloys Compds. 62 (2010) 25

Alloy selection: the NiAl-Mo system

3	4	5	6	7	8	9	10	11
Sc 1539	Ti 1670	V 1902	Cr 1857	Mn 1244	Fe 1540	Co 1495	Ni 1453	Cu 1083
Y 1526	Zr 1852	Nb 2467	Mo 2617	Tc 2200	Ru 2250	Rh 1963	Pd 1552	Ag 961
La 920	Hf 2227	Ta 3014	W 3407	Re 3180	Os 3027	Ir 2443	Pt 1772	Au 1065

Requisites

- High temperature oxidation resistance
- High thermal stability

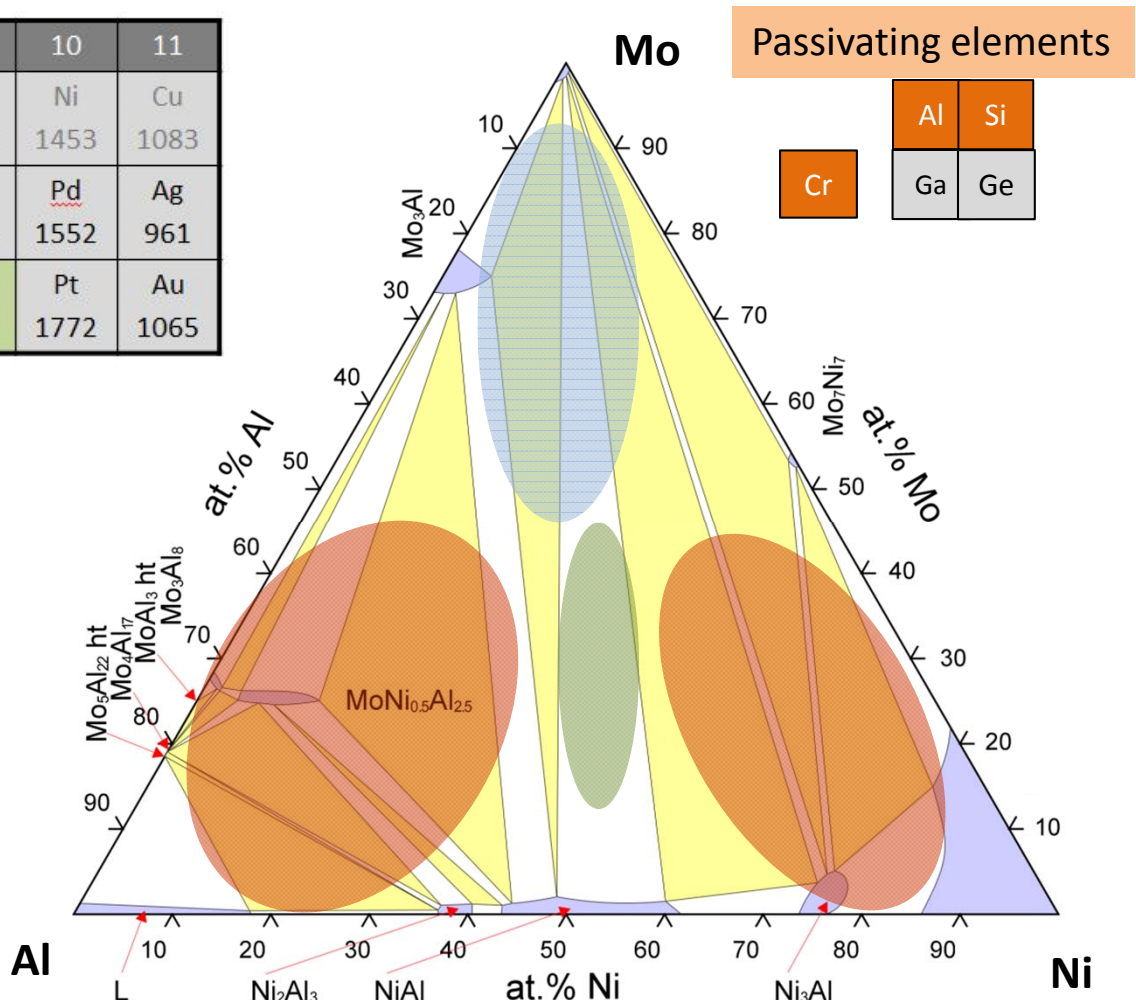
High melting + poor oxidation

Low melting + good oxidation

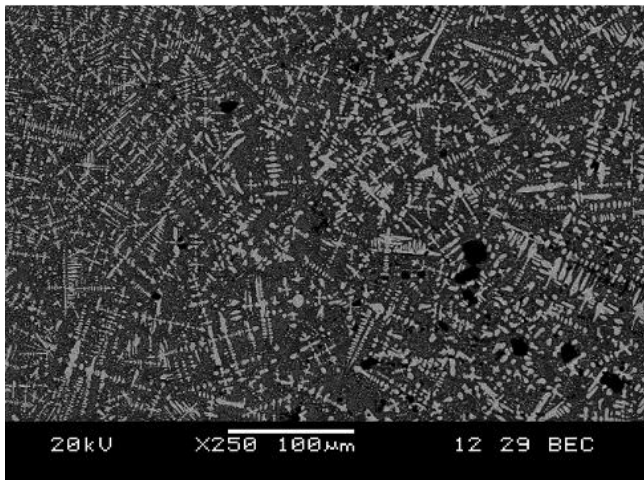
Mix of oxidation and melting & possibly creep strength

Haenschke et.al., J. Phys. 240(2010) 012063

Bei & George, Acta Mater 53(2005) 69



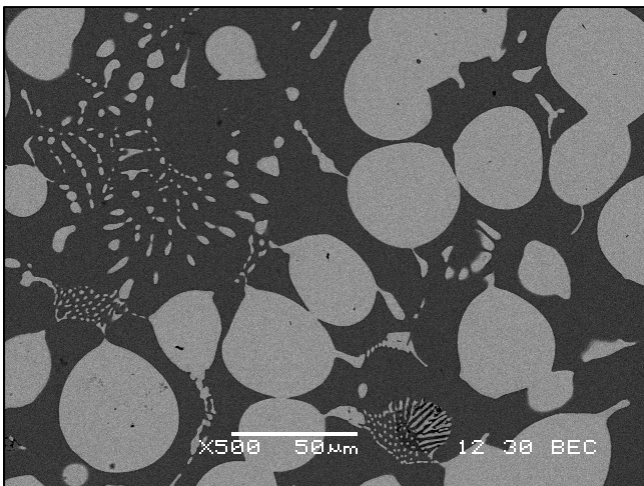
Processing and microstructures



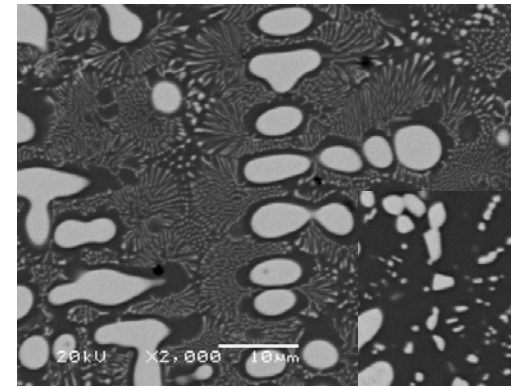
Arc-melted



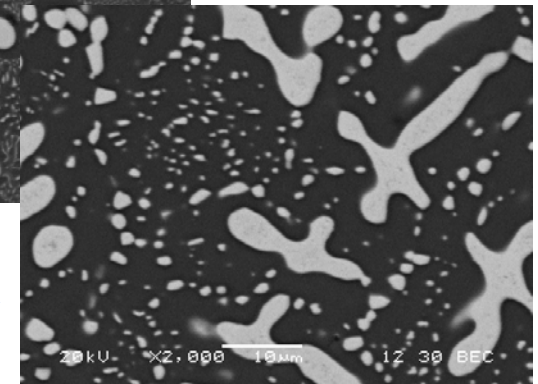
Directionally solidified



Liquid phase sintered



Stable microstructures
at 1500°C (12 hrs)



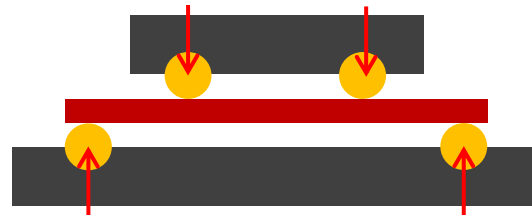
Fracture toughness of NiAl-Mo alloys

Mo forms the “backbone” for this alloy – creep and toughness

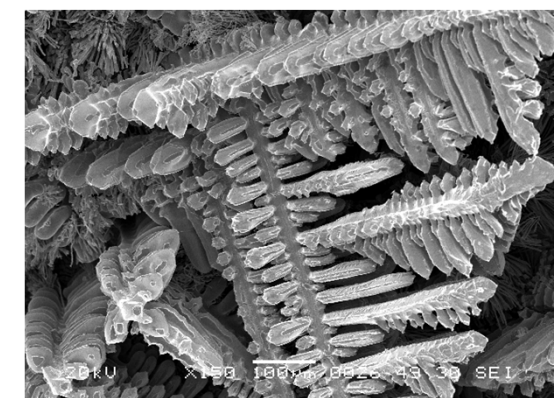
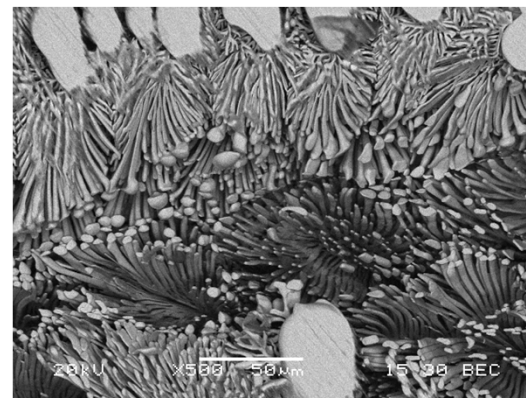
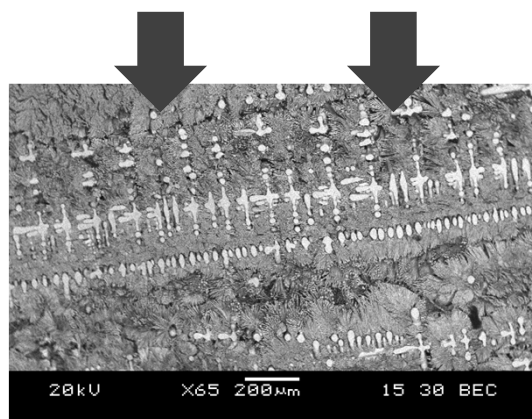
Toughness of NiAl $\sim 5 \text{ MPa}\cdot\text{m}^{1/2}$

Toughness of Mo-Si-B alloys $\sim 12 \text{ MPa}\cdot\text{m}^{1/2}$

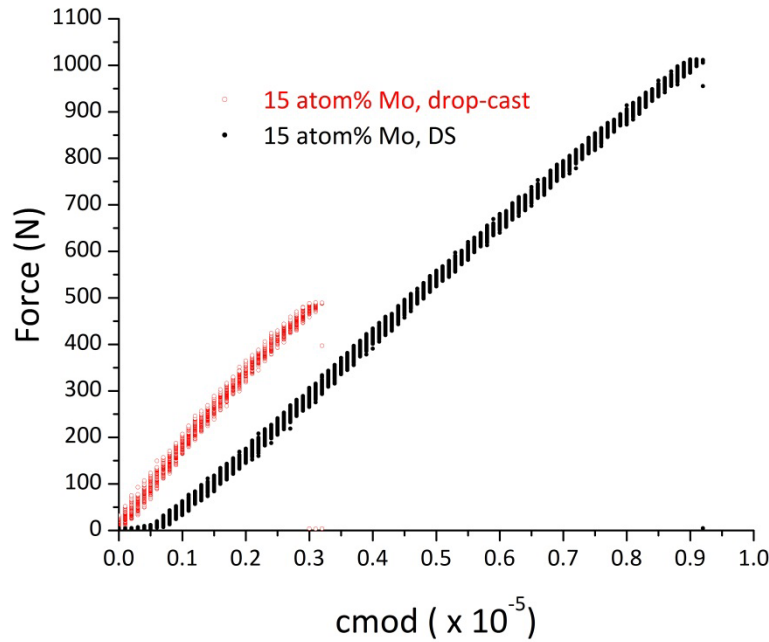
Fracture toughness ascertained using four point bending method



Force applied perpendicular to the growth direction [(0 0 1) direction]



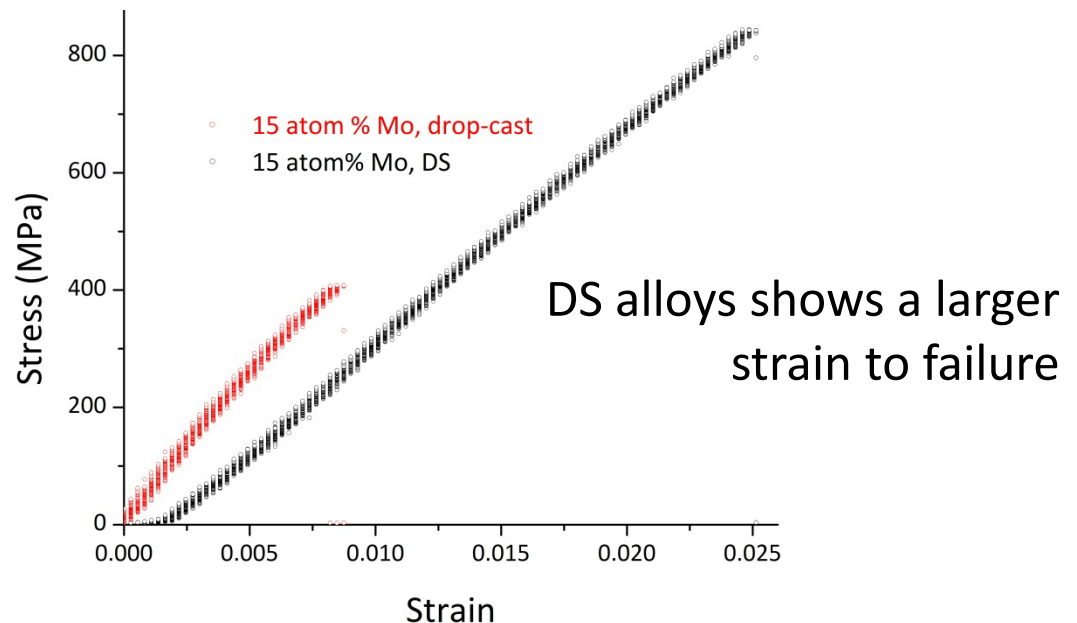
Fracture toughness of NiAl-Mo alloys



Flexural Strength
Drop-cast ~ 400 MPa
DS alloys ~ 850 MPa

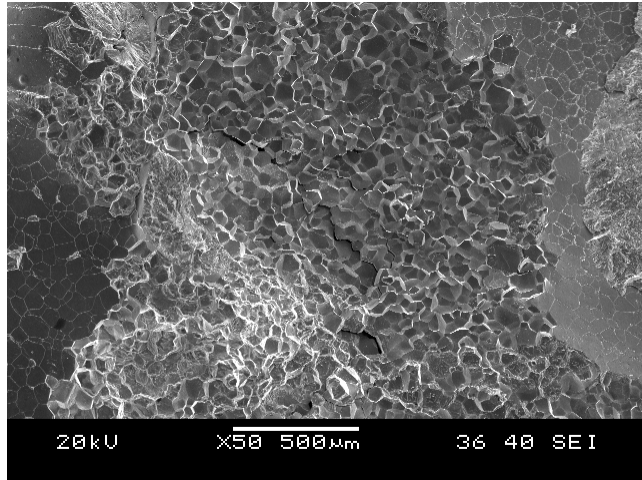
Fracture toughness of NiAl-
15%Mo [drop-cast] ~ 10
 $\text{MPa} \cdot \text{m}^{1/2}$
J. Kruzic, OSU

Fracture toughness of NiAl-
15%Mo [DS] $\sim 20 \text{ MPa} \cdot \text{m}^{1/2}$

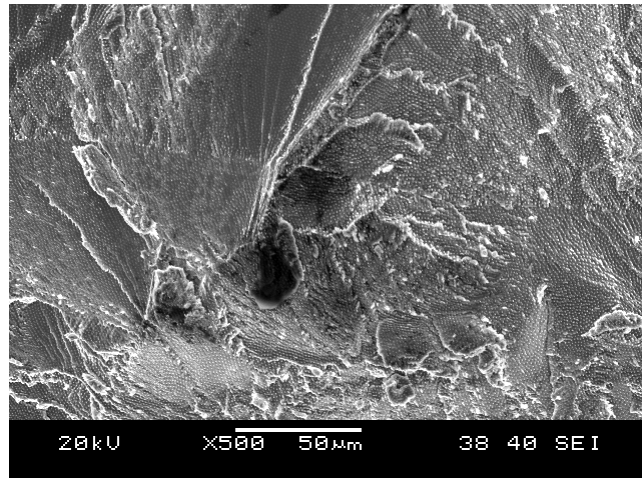


DS alloys shows a larger
strain to failure

Fracture toughness of NiAl-Mo alloys

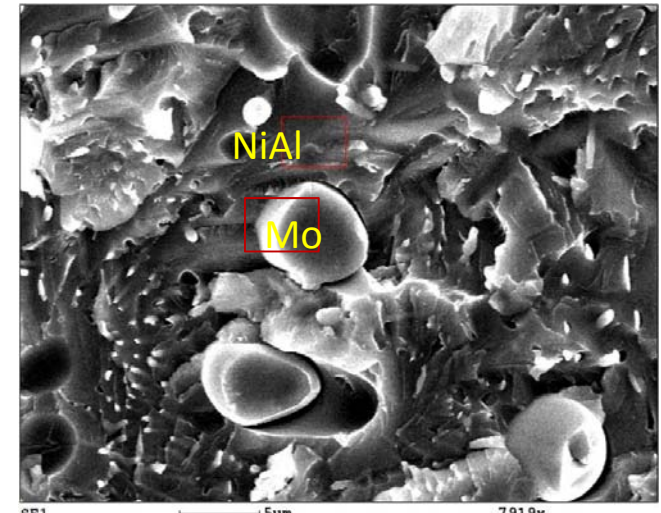


Fracture surface of drop-cast alloy ▲

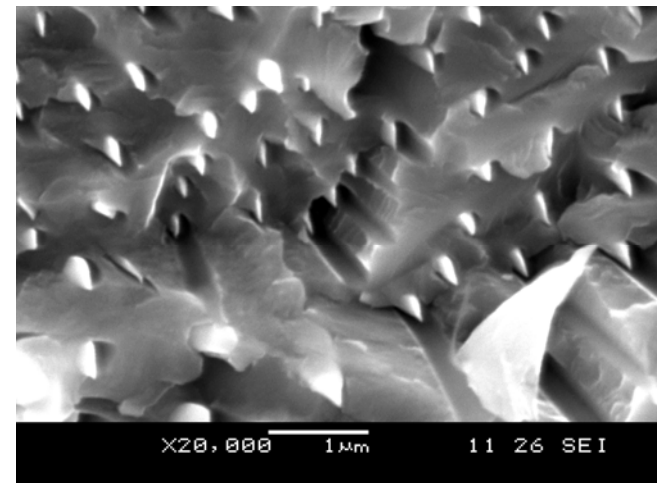


Fracture surface of DS alloy ▲

Presence of Mo dendrite pull-outs indicate a contribution towards toughening ▶

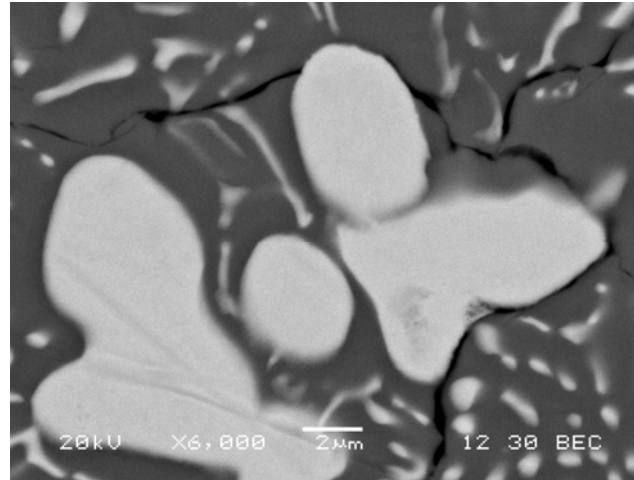
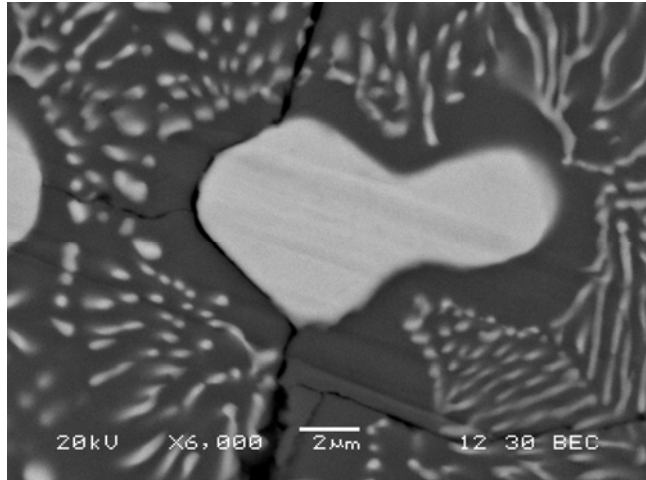


Some eutectic regions also showed the eutectic lamellae ▶ pull-outs

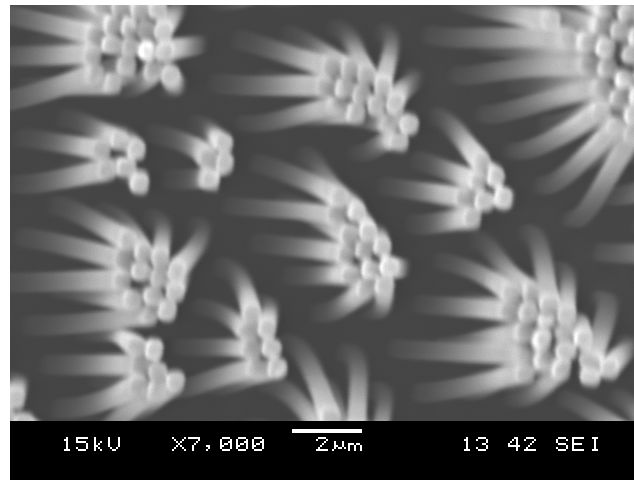
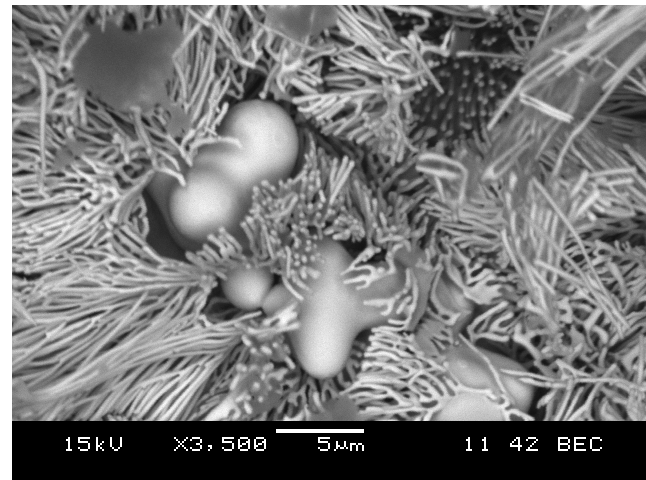


Bell et.al., article under preparation

Fracture toughness of NiAl-Mo alloys

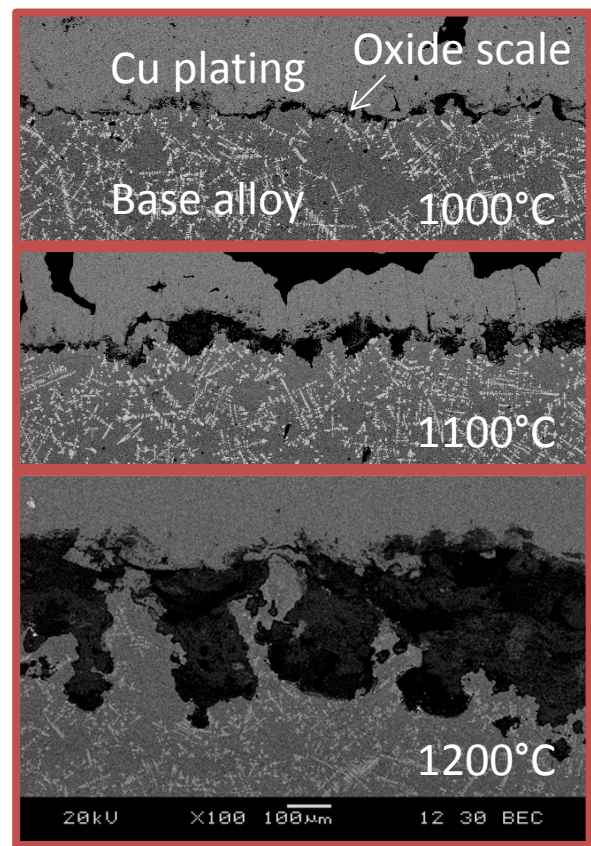
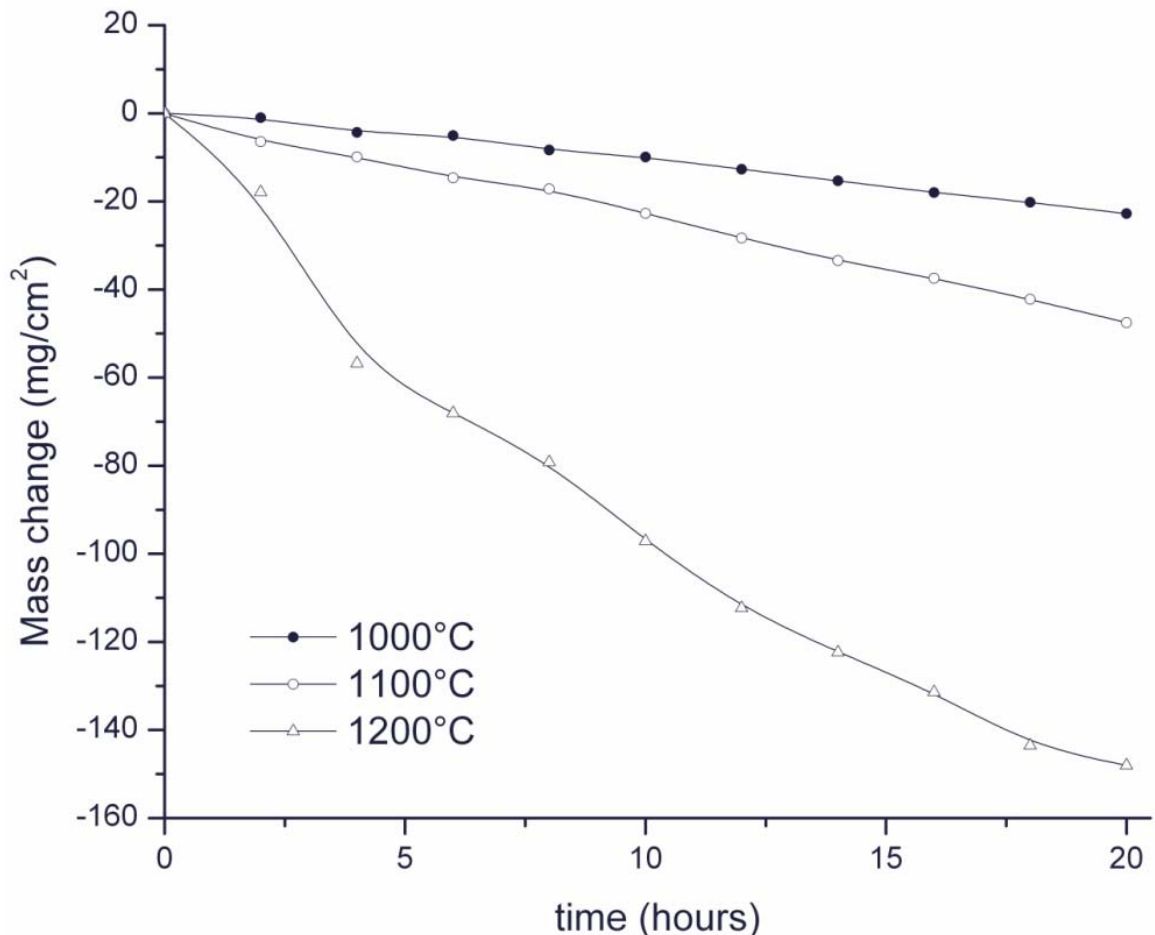


Mo serves to deflect
◀ crack path thereby
imparting
toughening



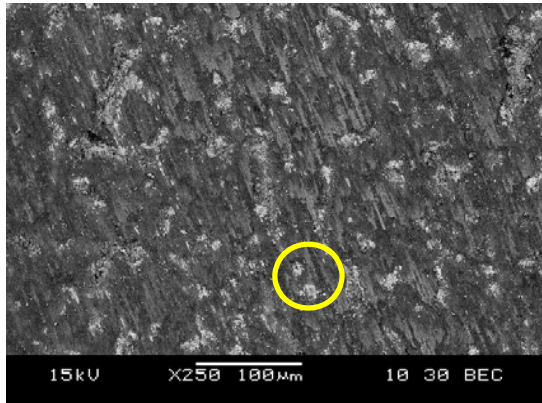
Mo additions also
◀ appear to induce a
small amount of
plasticity

Effect of temperature on oxidation

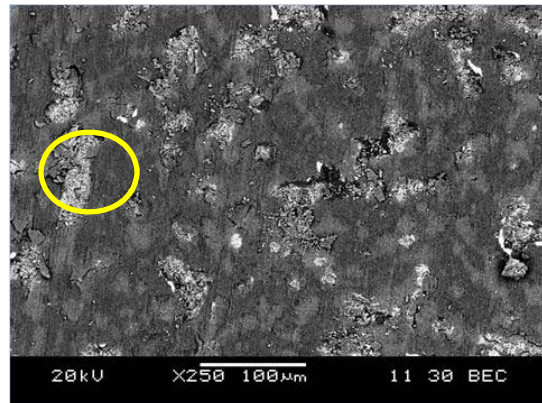


Ray et.al., Appl. Surf. Sci. 301(2014) 107

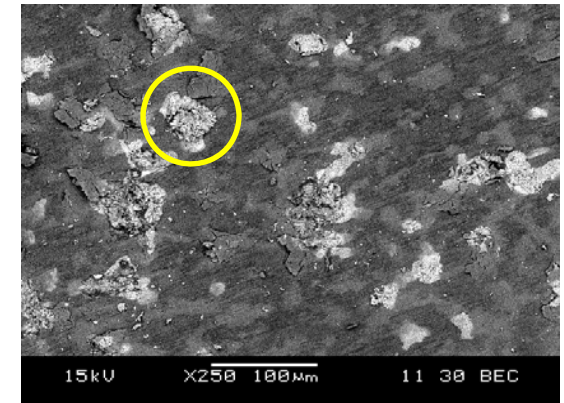
Evolution of the oxide scale with temperature



1000 °C



1075 °C

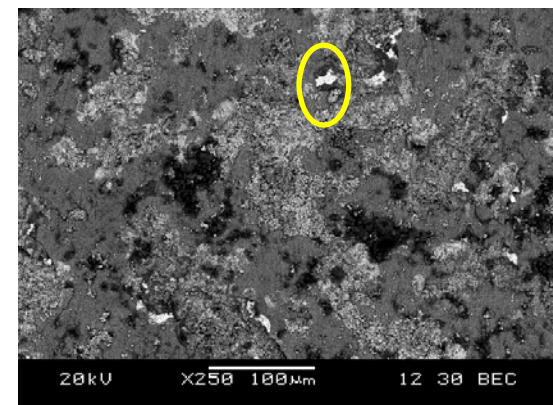


1100 °C

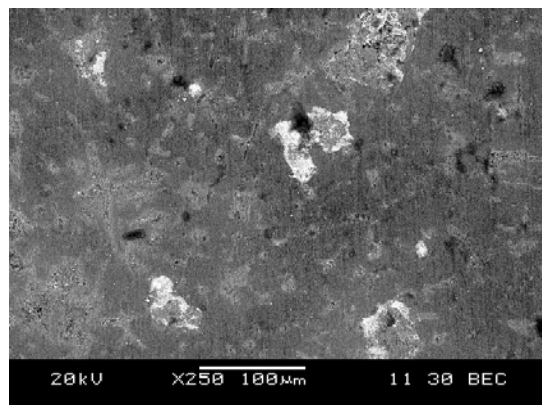
Oxidation time: 30 minutes

As temperature increases,
 NiMoO_4 regions grow larger,
but they start disappearing
above 1100 °C

NiAl_2O_4 and NiO seem to
predominate above 1125 °C

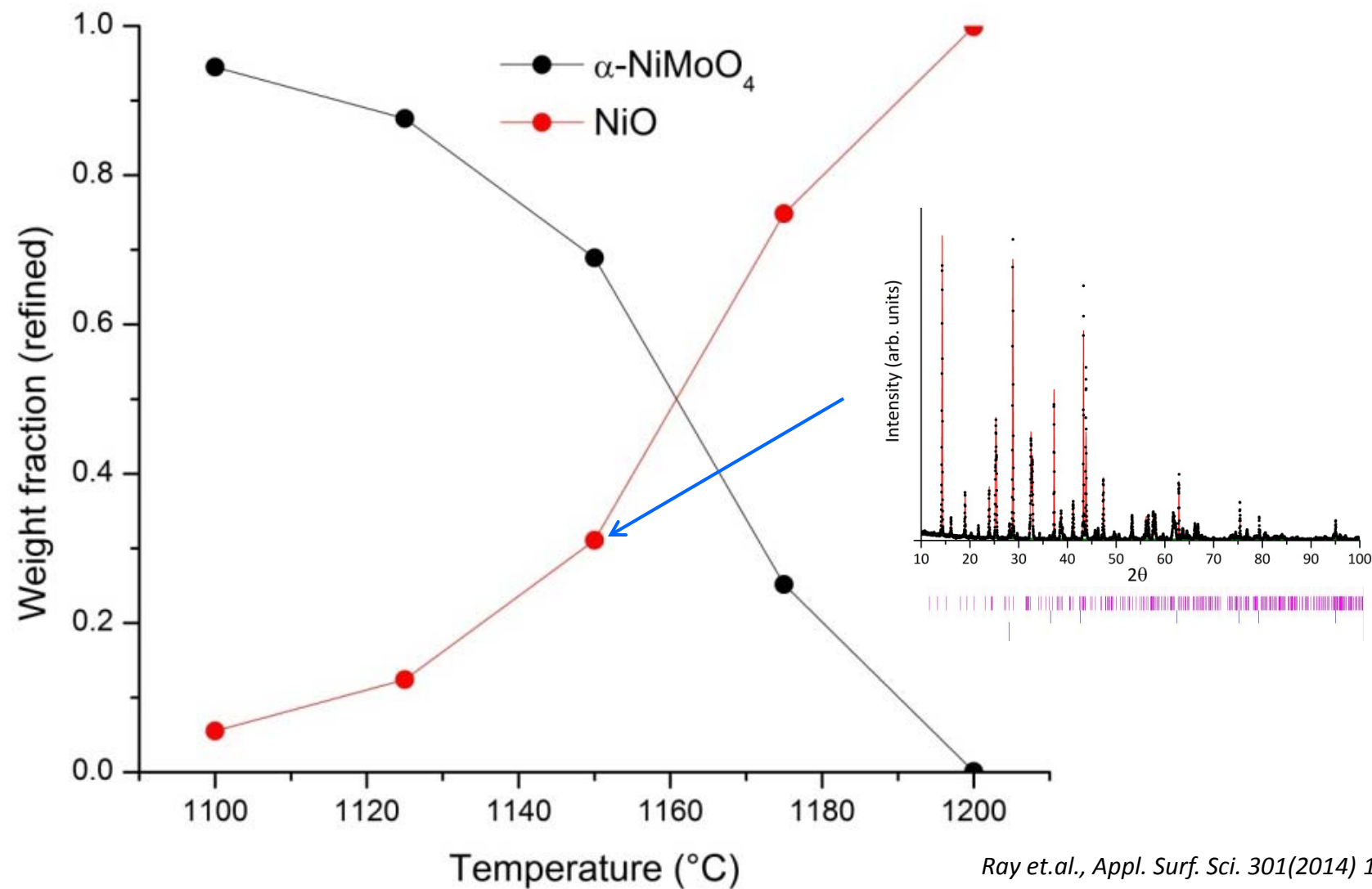


1125 °C



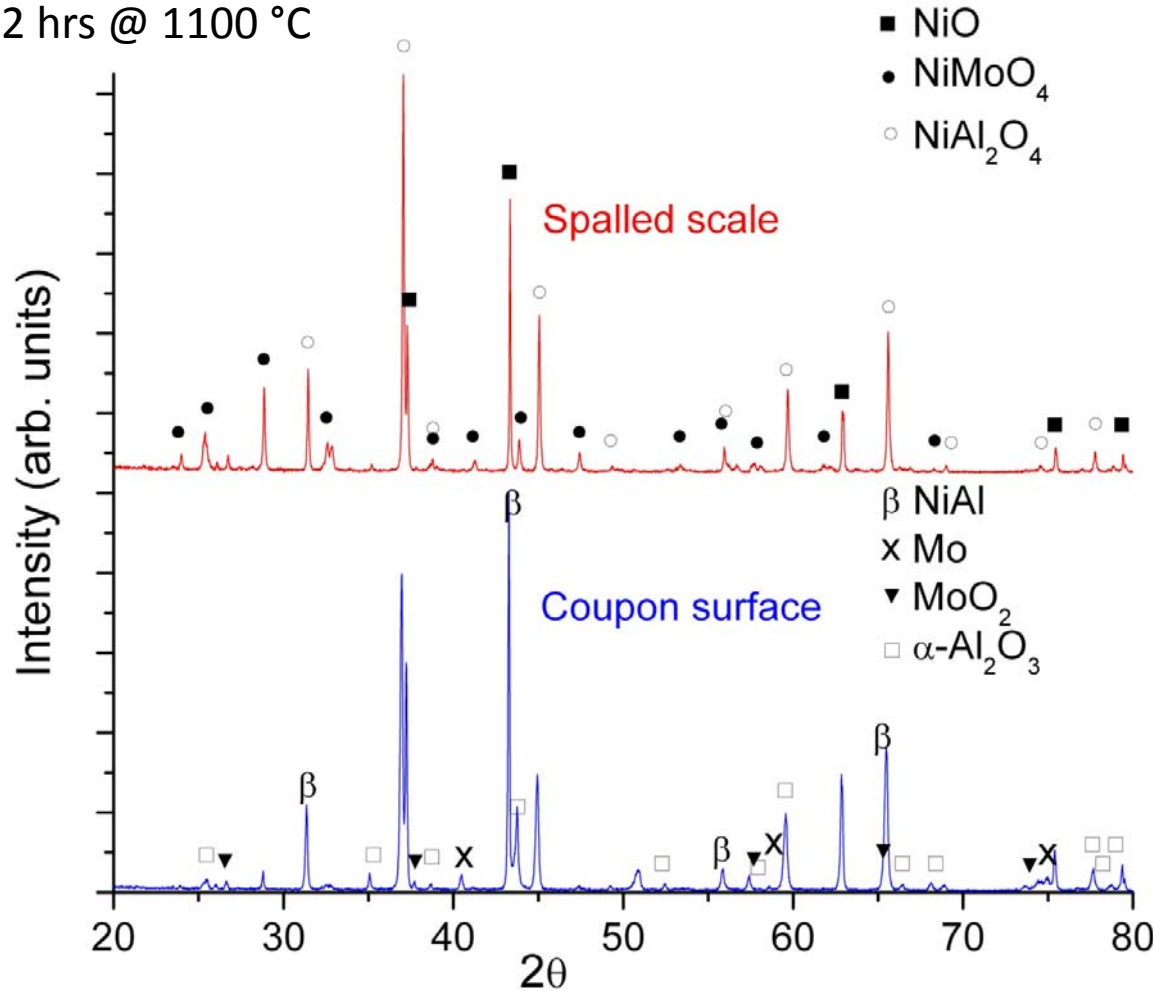
1200 °C

Stability of NiMoO_4



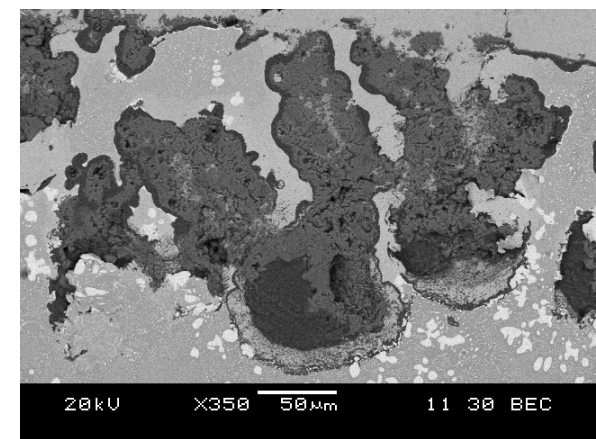
Comparisons – spalled vs adherent scale

2 hrs @ 1100 °C



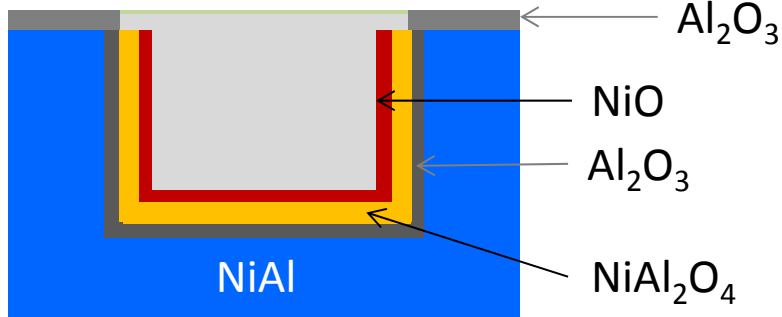
Major differences –

- The amount of NiMoO₄ and NiO is drastically reduced in the coupon surface
- The α-Al₂O₃ and MoO₂ are virtually absent in the spalled scale.
- NiAl₂O₄ shows up in both cases as a major phase.



Ray et.al., Appl. Surf. Sci. 301(2014) 107

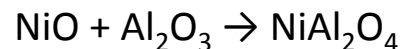
A physical model for oxidation



NiMoO₄ dissociates progressively



The NiO reacts with the underlying Al₂O₃ to form the spinel interphase



NiMoO₄ dissociates: poor oxidation;
NiMoO₄ doesn't dissociate: $\beta \rightarrow \alpha$
transformation with 20% volume change

Consider the oxidation of a Mo rich region of the surface.

Initial oxidation of Mo results in the formation of MoO₃ which later volatilizes.

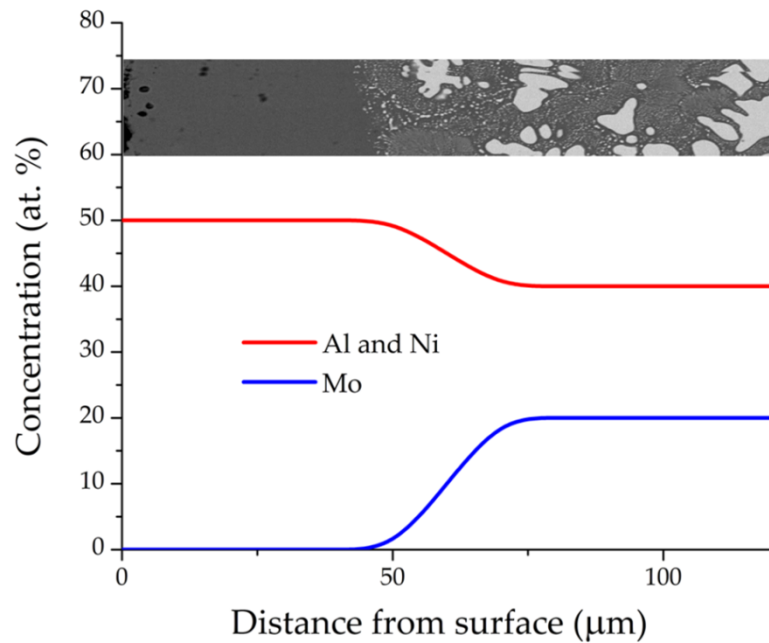


NiMoO₄ forms at the interface along with alumina



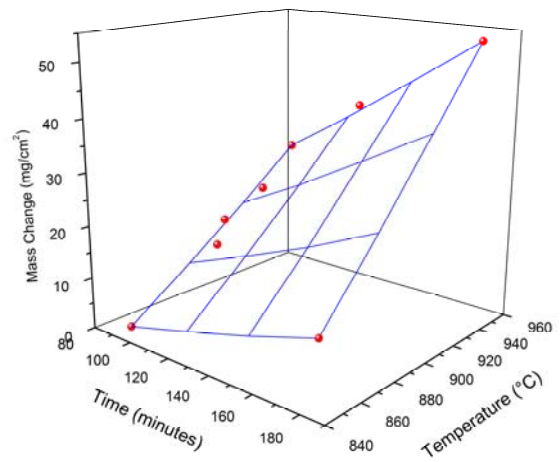
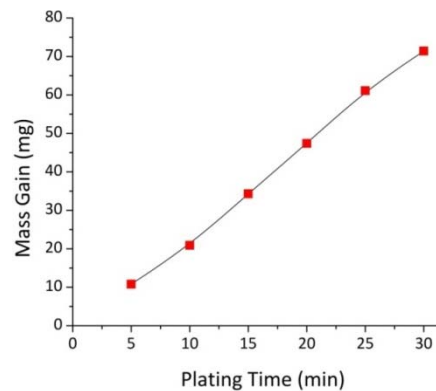
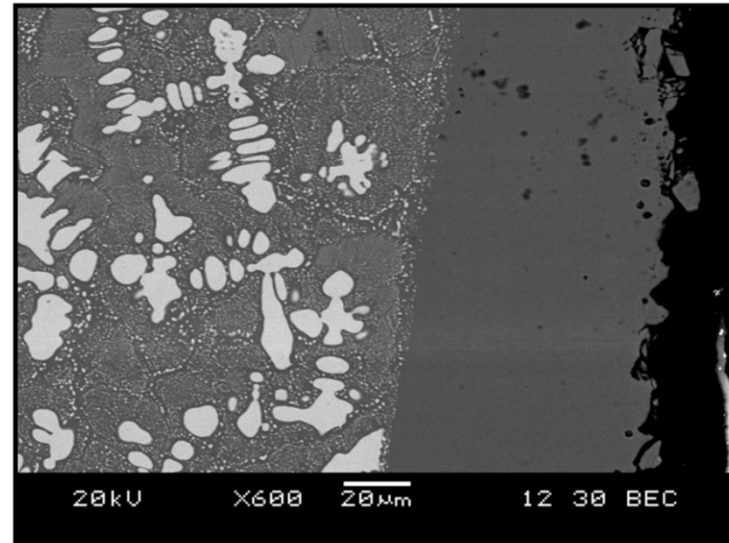
Ray et.al., article under preparation

Coating methodologies

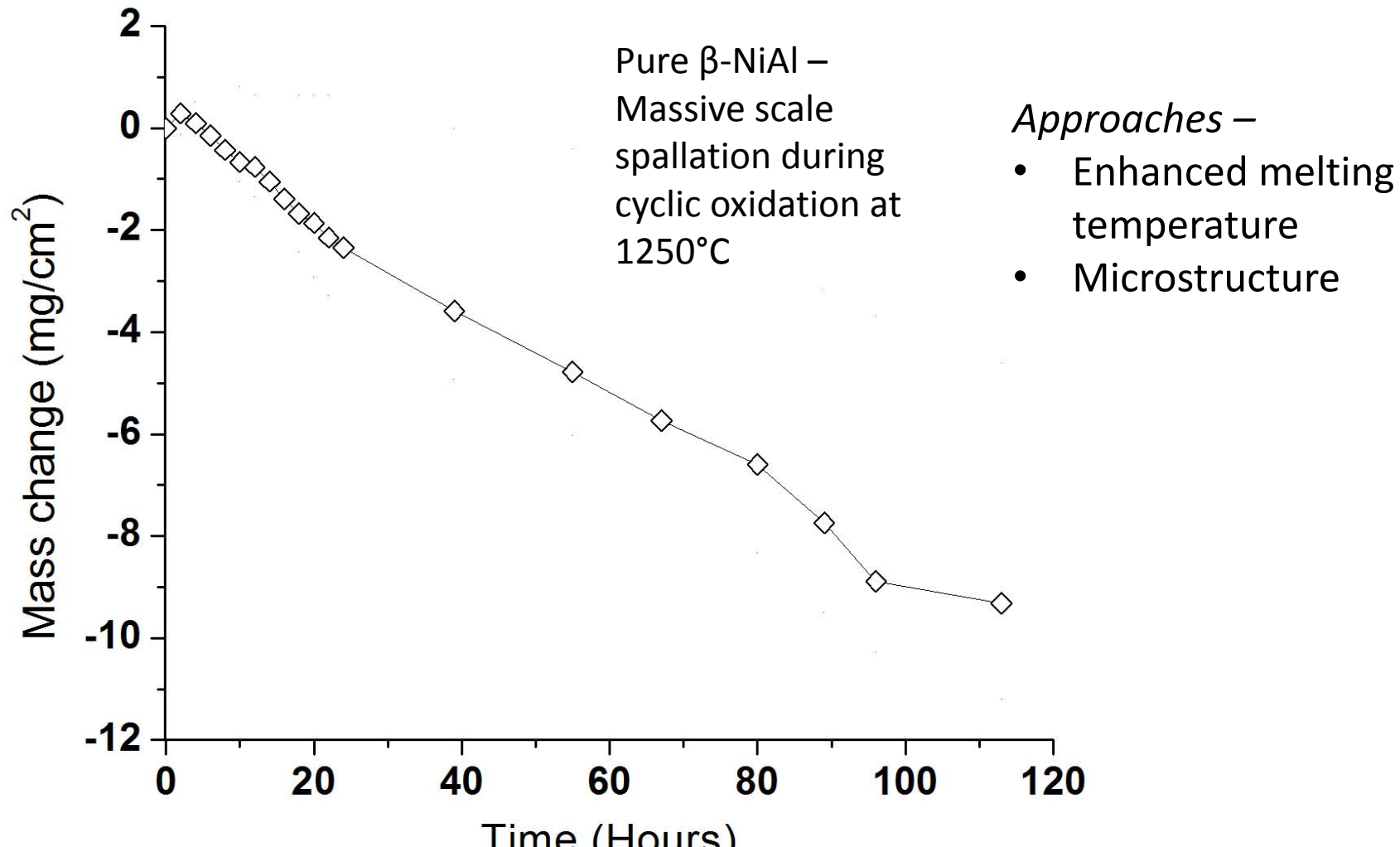


Coating process: Electrodeposition(Ni) and pack cementation (Al); anneal at 1350°C for 2 hours

Accurate statistical models of electroplating and pack cementation for controlling thickness

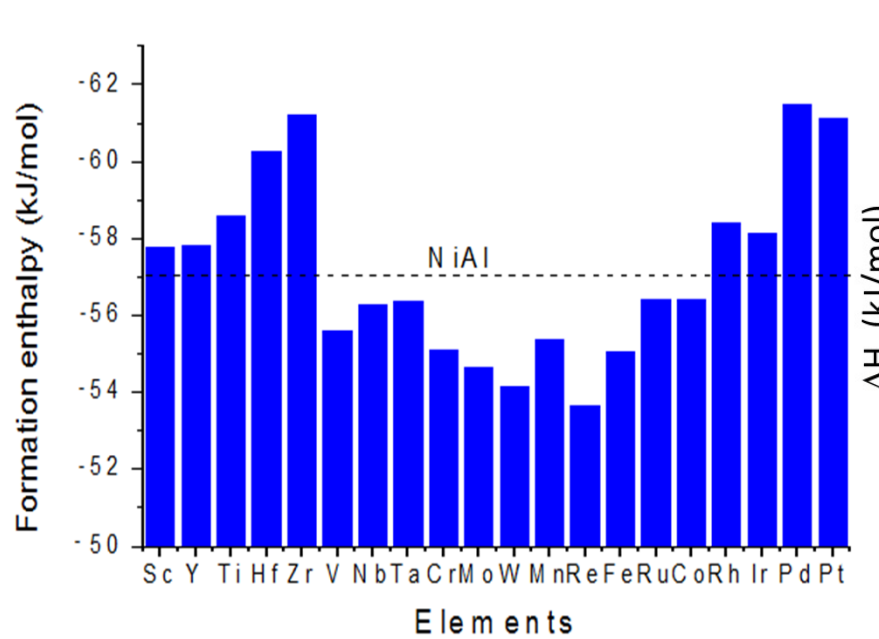


Oxidation of NiAl



Ray et.al., JOM 62 (2010) 65

Alloying additions: computational screening

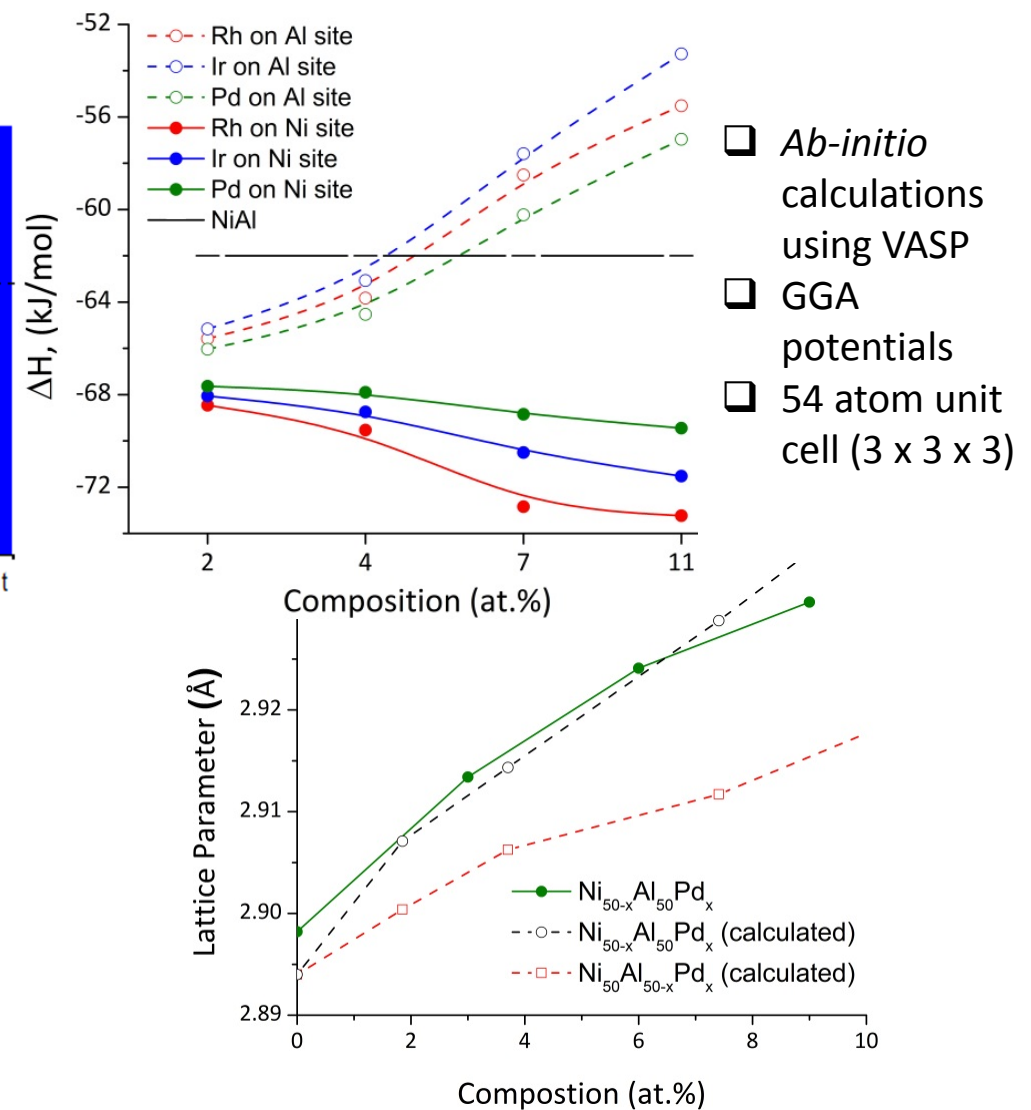


Brammer et.al., Adv. Sci. Tech. 72 (2010) 31

$$T_m = 0.032 \frac{E^c}{k_B}$$

Rose-Ferrante
theory of Universal
Binding Curve

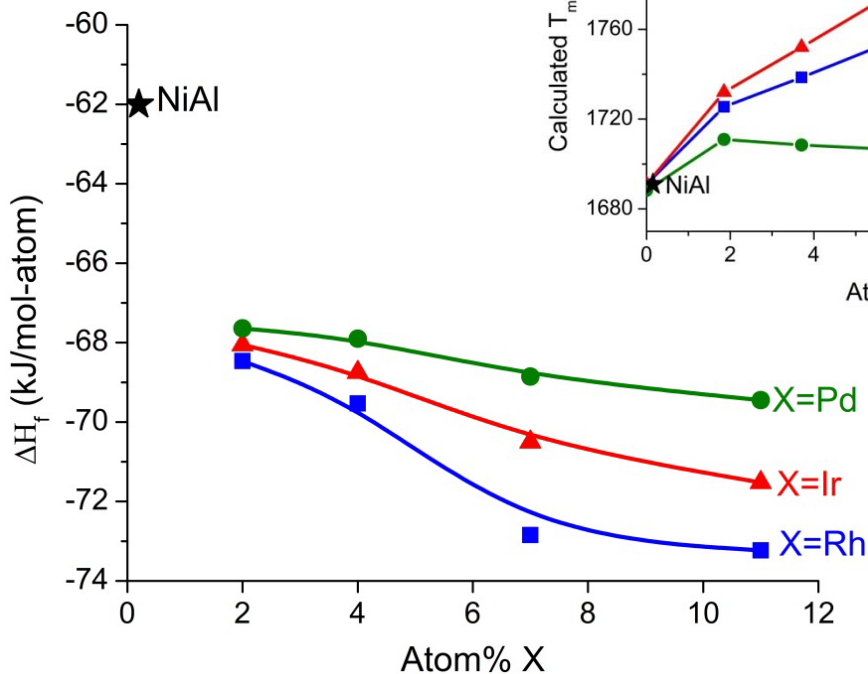
$$E^c = x_1 E_1^c + x_2 E_2^c + x_3 E_3^c - \Delta H_f$$



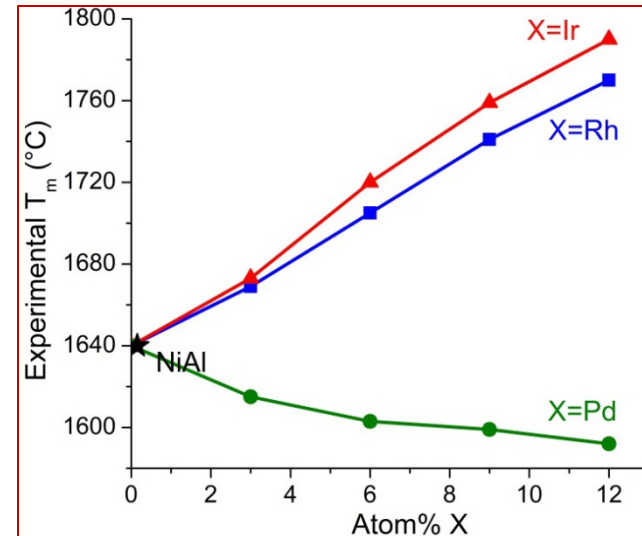
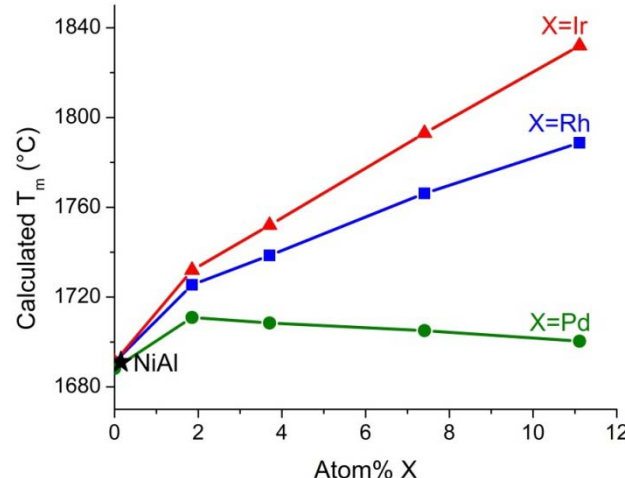
Ab-initio studies on the role of PGM additions

$$T_m = 0.032 E^c / k_B$$

$$E^c = x_1 E_1^c + x_2 E_2^c + x_3 E_3^c - \Delta H_f$$

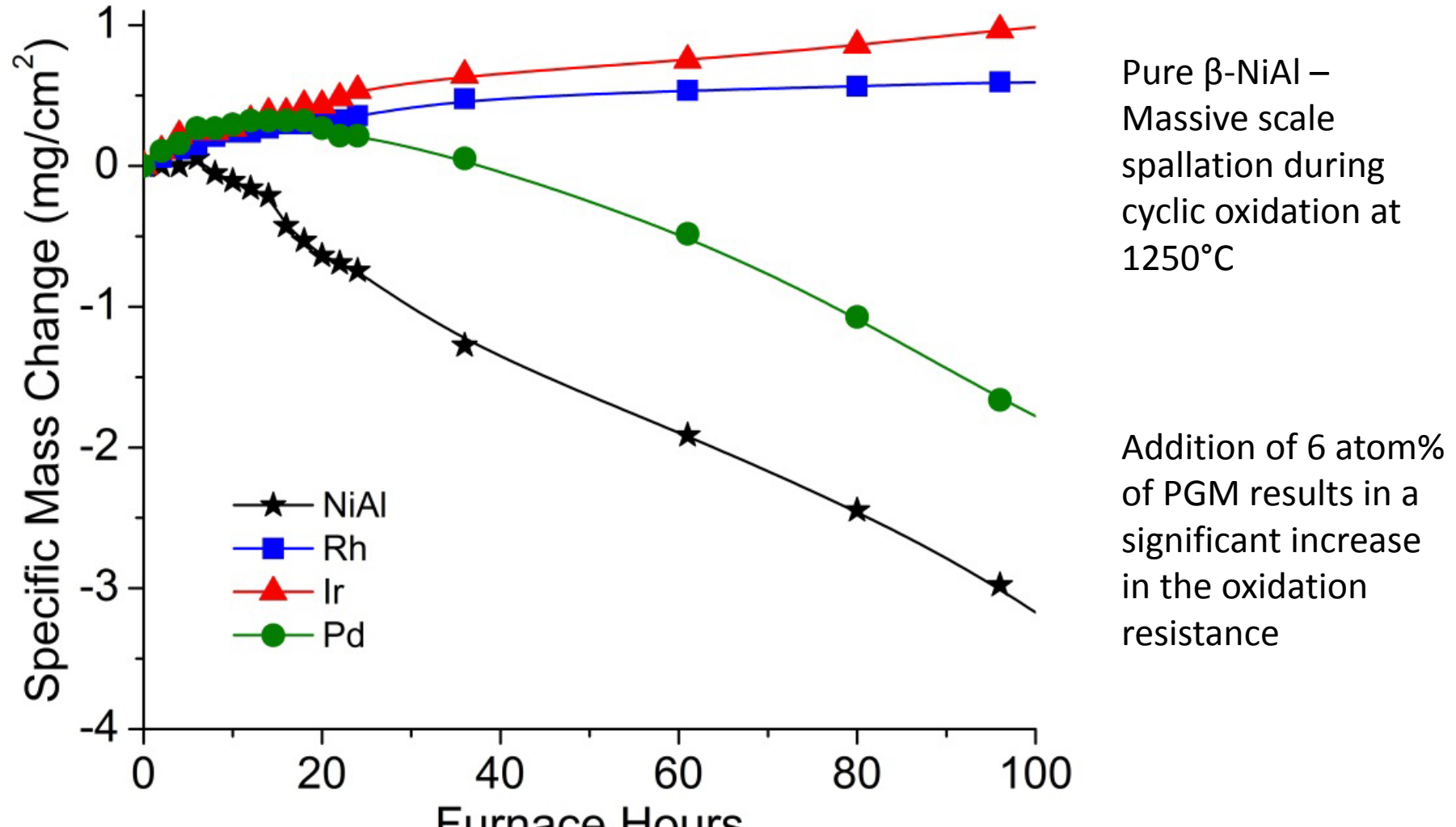


Formation enthalpies estimated using
the VASP code with GGA potentials



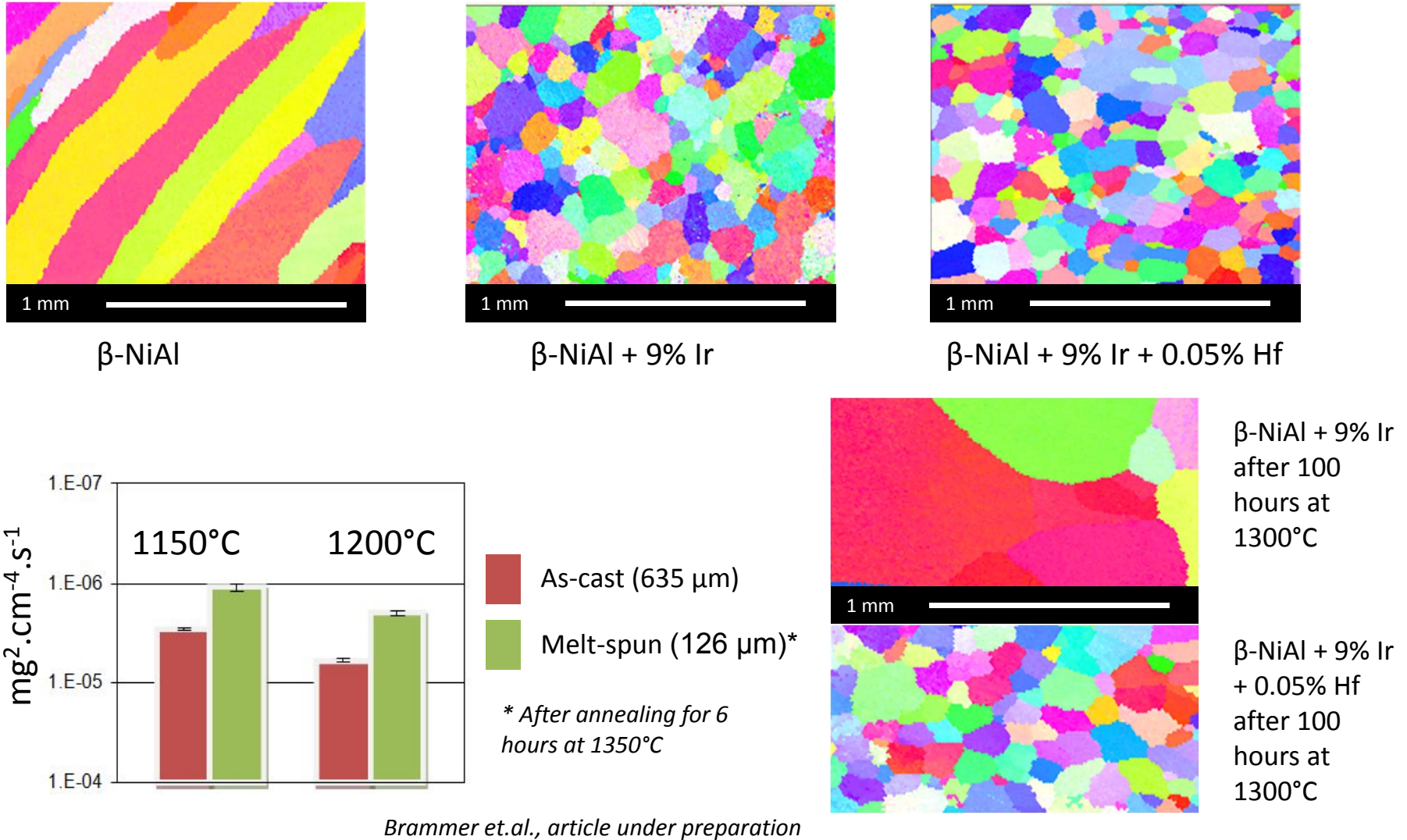
Metal	Cohesive E (kJ/mol)	Metal	Cohesive E (kJ/mol)
Al	327	Ir	670
Ni	428	Pd	376
Rh	554		

Effect of PGM additions on oxidation

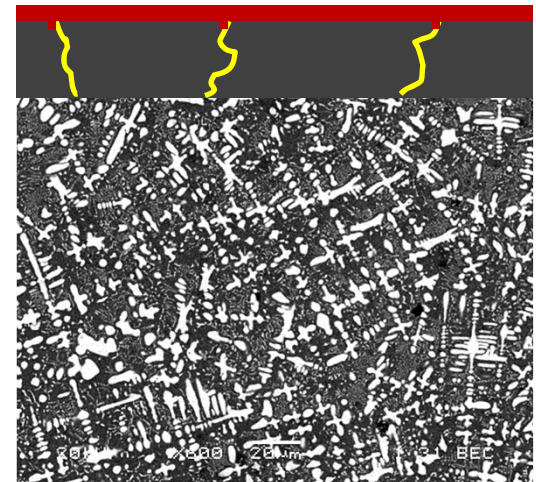
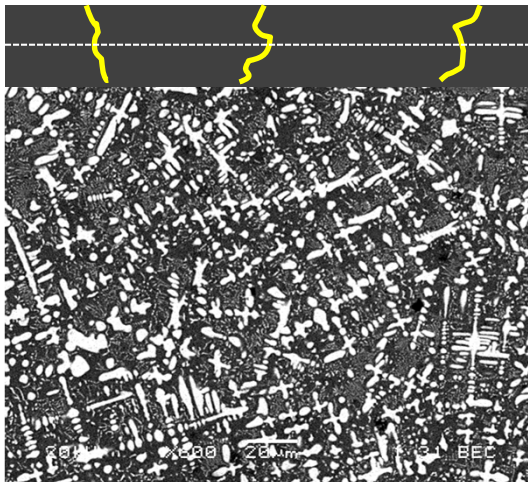
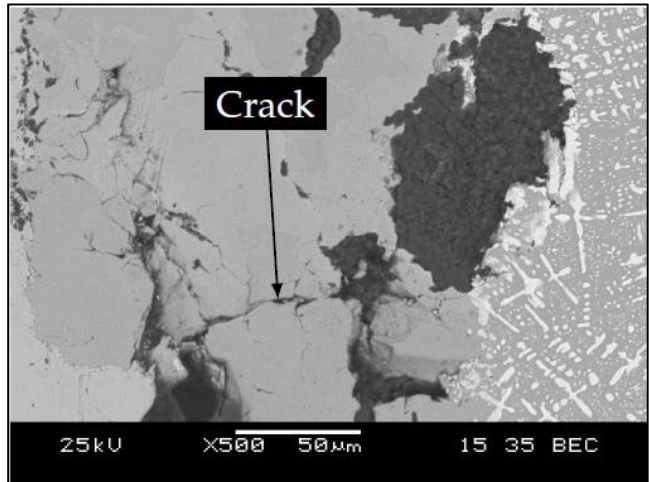


Ray et.al., JOM 62 (2010) 65

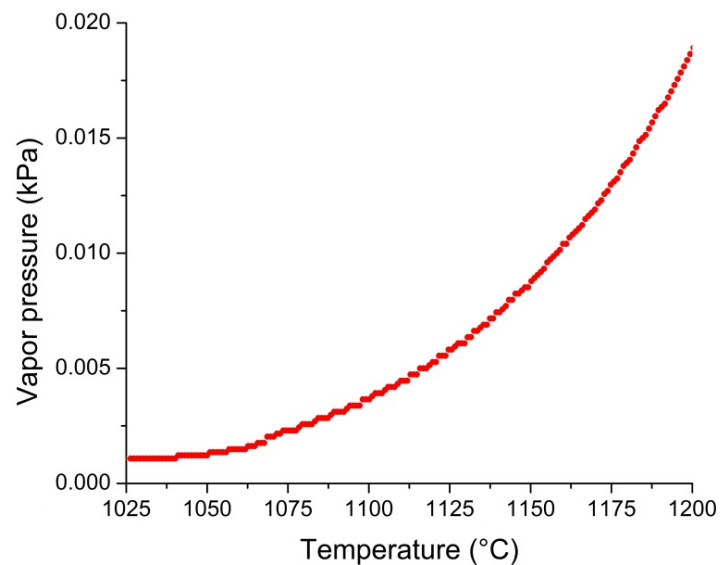
The role of grain size



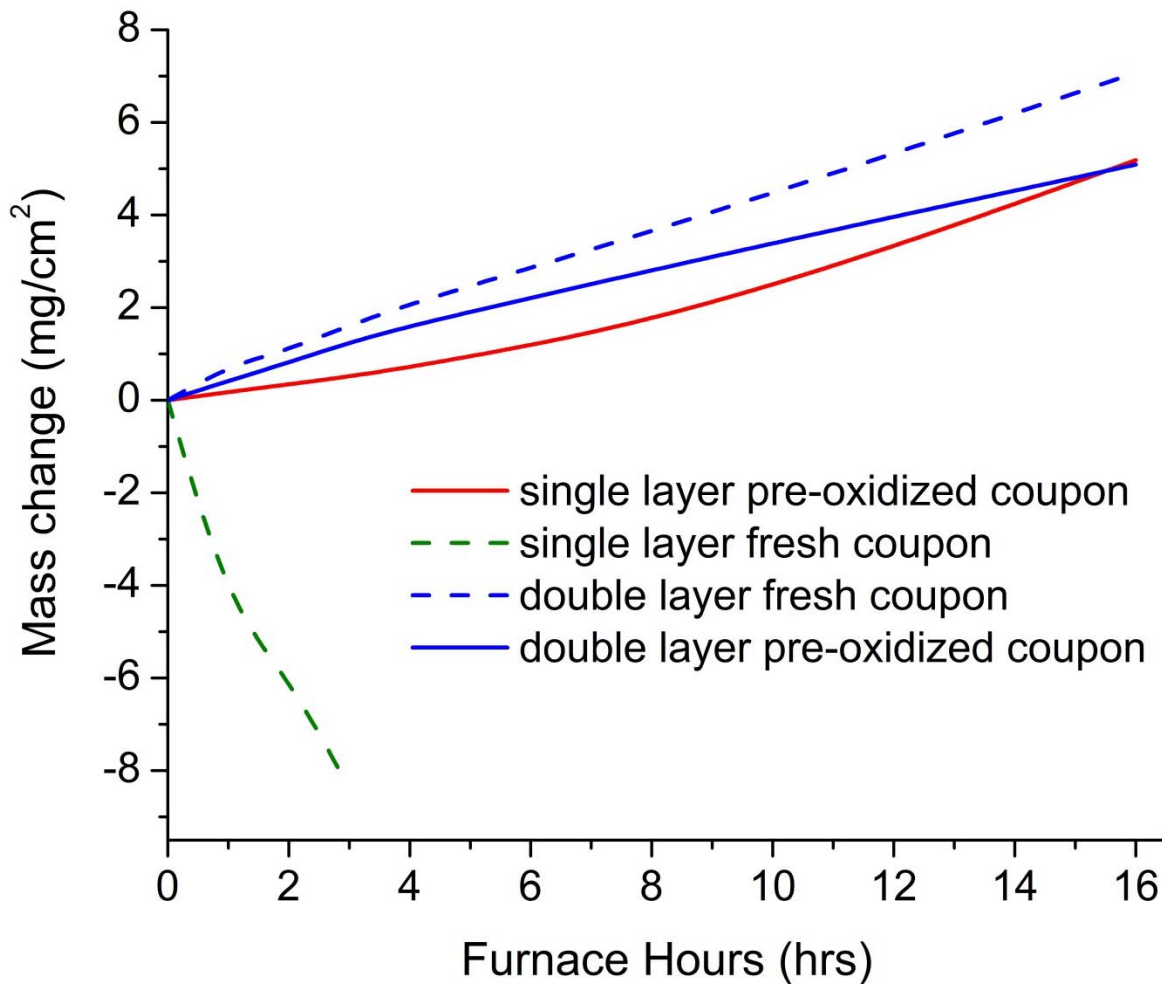
Failure mechanisms for the coatings



- Pre-existing cracks provide oxidation pathways.
- Integrity is a function of NiMoO_4 formation vs Al_2O_3 coverage.
- T dependence is function of Al_2O_3 growth rate and MoO_3 vapor pressure



Oxidation behavior of coated alloys 1150°C



Optimal coating approach:

Double layered coatings

Pre-oxidized at 1100°C for 5 hours

Bell et.al., article under preparation

Perspectives

- Semi-empirical techniques assisted in initial selection; further work resulted in an alloy with high melting temperature and adequate toughness, with oxidatively stable coatings.
- Computational methods were not used for down-selecting materials on the basis of oxidation resistance, due to a relatively small playground once criteria for high melting temperature and tough “backbone” phase were fulfilled

Expanding the toolbox

- Need for more accurate models for materials genomics, especially with multiple principal components which presents a greater complexity of challenges
- Standard DFT based approaches are more suited to ordered materials rather than disordered solid solutions like HEAs
- Looking ahead – use computational tools for oxidation resistance, while selecting alloy systems that retain structural stability with temperature (**Entropically Stabilized Alloys – studied using KKR-CPA**) when oxidized (system selection using new computational tools – GSSNEB)

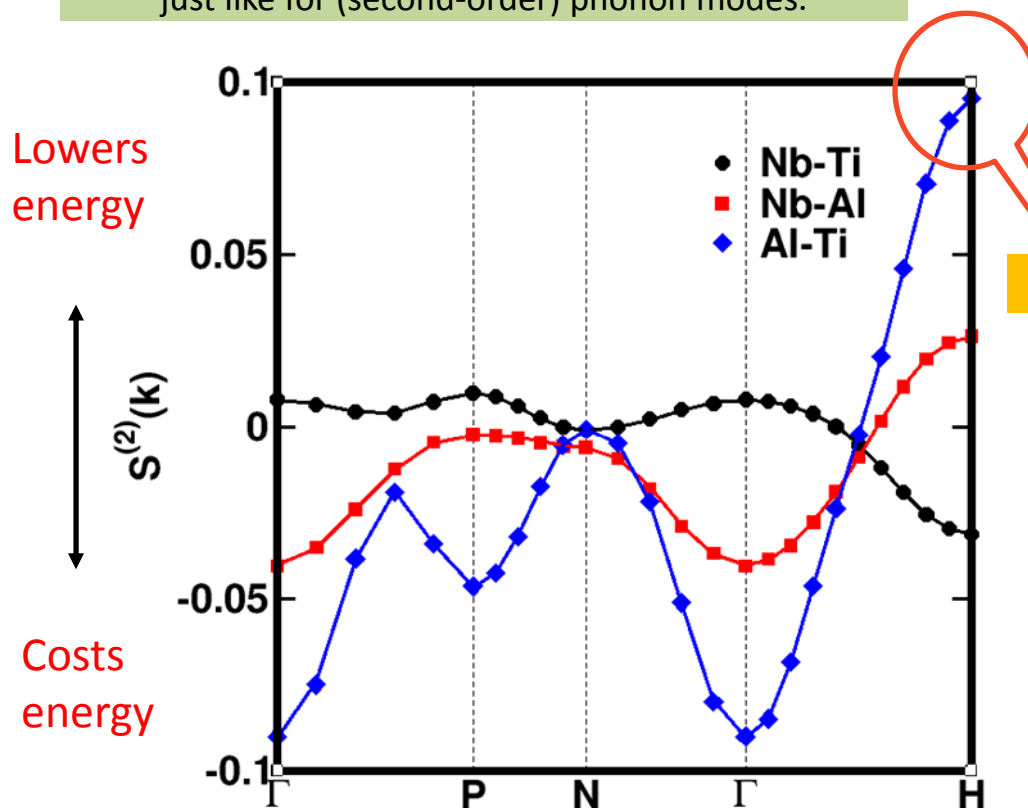
Short Range Ordering in N-component Alloy

- Atomic SRO can be calculated using *all-electron, first-principles KKR-CPA-based linear-response code* addressing inhomogeneous chemical fluctuations.
- We can uniquely identify atomic SRO in alloy using **Concentration Wave analysis** using an analytic N-dimensional transform for Gibbs' (chemical) space.
- Approach was tested and verified on
 - Ternary A2 (bcc) $\text{Nb}_{25}\text{Al}_{25}\text{Ti}_{50}$
 - Quinary A1 (fcc) $\text{Ni}_{20}\text{Cu}_{20}\text{Al}_{20}\text{Ti}_{20}\text{Zr}_{20}$

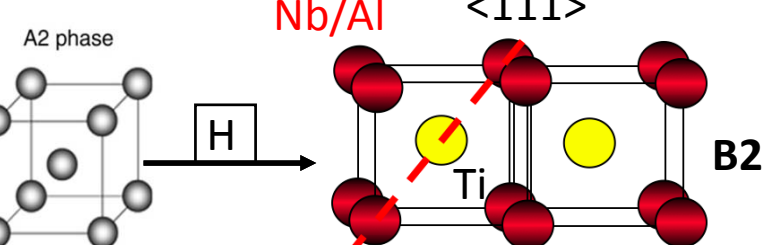
$Ti_{50}Nb_{25}Al_{25}$: SRO unstable eigenmodes

SRO indicate the unstable chemical modes

All mode determined simultaneously,
just like for (second-order) phonon modes.



Alloy-specific partially-ordered B2 phase



Strong partially-ordered B2 (H-pt) ordering

First unstable mode (H-point)
 $k_0 \rightarrow <100> = <111>$

Temperature Scale

Theory spinodal $T_{sp} = 1750$ K

Experimental B2 order: 1713 K

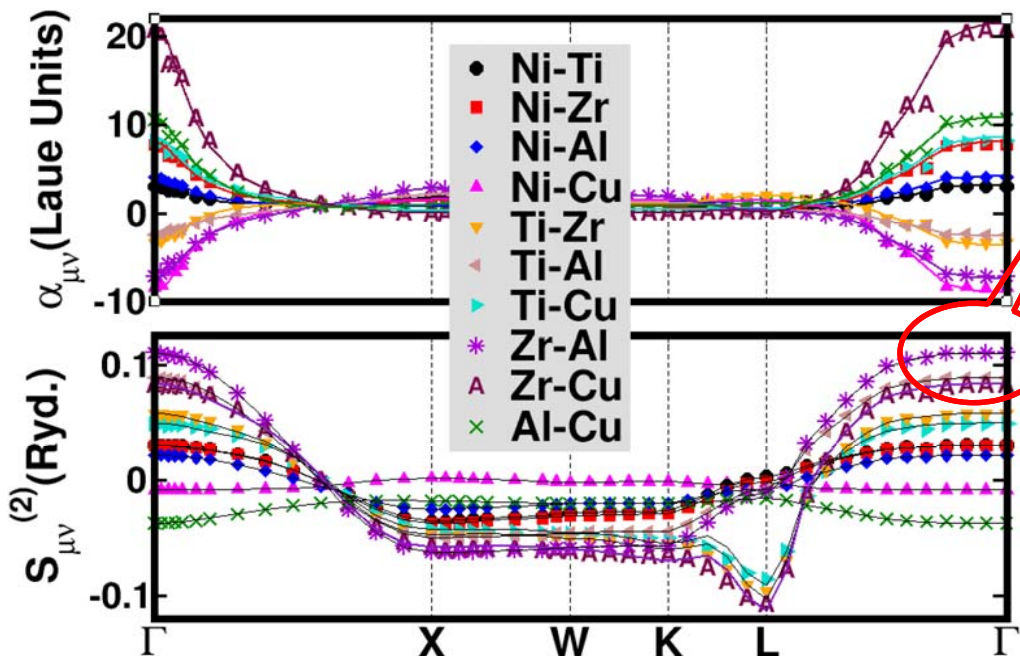
D.D. Johnson et al., Phil Mag. Lett 79, 551 (1999)

SRO in Quinary NiTiZrAlCu

Direct Calculation KKR-CPA
Formation Energy = +16.4 mRyd
 $T_c = 1610$ K

Experimental findings – HEA by MA, multiphase intermetallics by casting

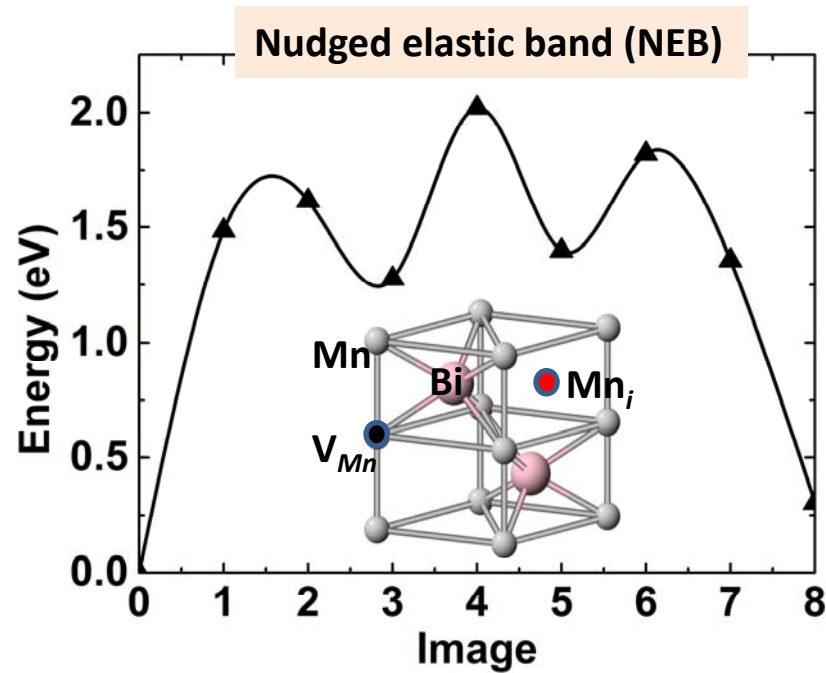
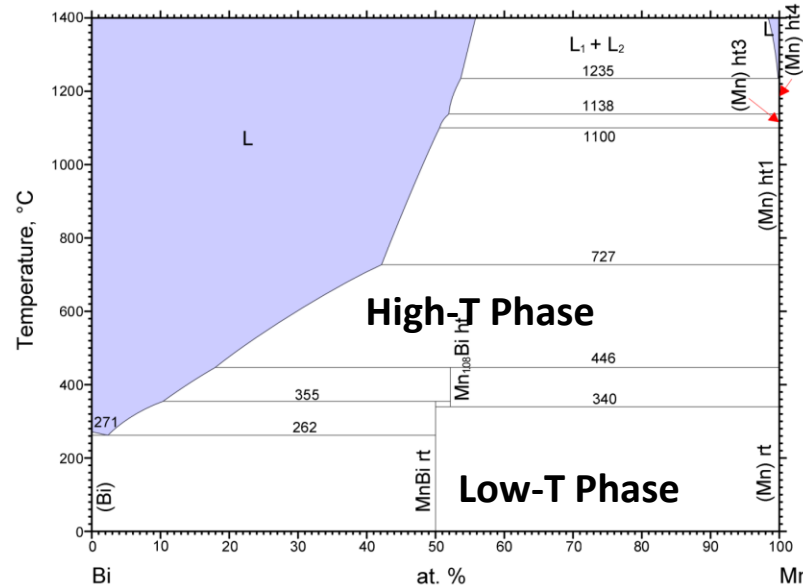
SRO: $k_0 = [000]$ Clustering
SRO: Unstable Modes (Zr-Cu)
 $S^{(2)}$: competing Zr-Al,Zr-Cu,Ti-Al
 $T_{sp} = 1510$ K (estimated)



Real Space decomposition of $S^{(2)}$ upto 5-shells.

Shell _{RS} /Modes	Zr-Al	Zr-Cu	Ti-Al
$S_0^{(2)}$	+10.4	+9.39	+8.55
$S_1^{(2)}$	-0.07	+2.37	-0.55
$S_2^{(2)}$	-0.01	-1.92	-0.05
$S_3^{(2)}$	-0.10	-4.27	+0.12
$S_4^{(2)}$	-0.01	+0.50	-0.01

Kinetic Barriers for MnBi: HTP to LTP



- In HTP, interstitial Mn couples anti-ferromagnetic and reduces magnetization
- Interstitial-vacancy pair (Mn_i - V_{Mn}) only costs 0.3 eV when separated by 1 atom.
- **Barrier in between is as high as 1.7-2 eV, which limits kinetic for HTP \rightarrow LTP**
- Kinetically stable HEA desirable for mechanical properties.

Summary

